



**HAL**  
open science

## Simultaneous enzyme grafting on bio-inspired scaffolds for antibacterial protection

Baptiste Arbez, Chloé Retourney, Fabienne Quilès, Gregory Francius, Henri-Pierre Fierobe, Sofiane El-Kirat-Chatel

### ► To cite this version:

Baptiste Arbez, Chloé Retourney, Fabienne Quilès, Gregory Francius, Henri-Pierre Fierobe, et al.. Simultaneous enzyme grafting on bio-inspired scaffolds for antibacterial protection. *Materials Advances*, In press, 10.1039/d3ma00703k . hal-04398415

**HAL Id: hal-04398415**

**<https://hal.univ-lorraine.fr/hal-04398415>**

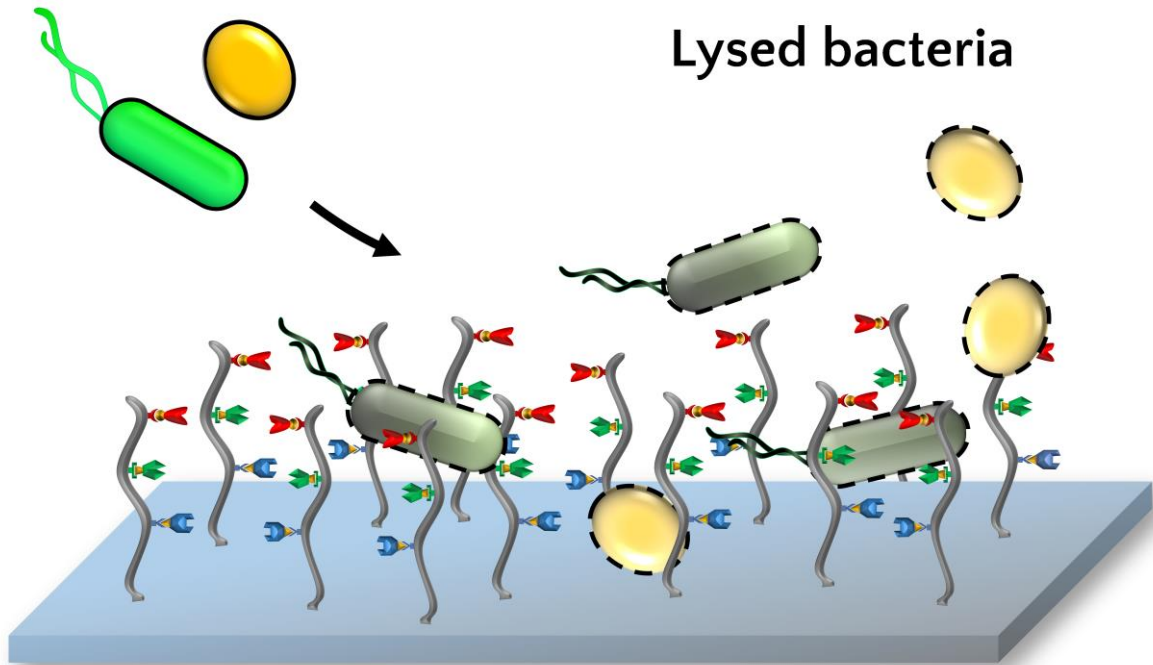
Submitted on 16 Jan 2024

**HAL** is a multi-disciplinary open access archive for the deposit and dissemination of scientific research documents, whether they are published or not. The documents may come from teaching and research institutions in France or abroad, or from public or private research centers.

L'archive ouverte pluridisciplinaire **HAL**, est destinée au dépôt et à la diffusion de documents scientifiques de niveau recherche, publiés ou non, émanant des établissements d'enseignement et de recherche français ou étrangers, des laboratoires publics ou privés.

1

2 GRAPHICAL ABSTRACT



**Bio-inspired multienzymatic scaffold**

3

4

5 Simultaneous enzymes grafting on bio-inspired  
6 scaffolds for antibacterial protection

7 Baptiste Arbez<sup>a</sup>, Chloé Retourney<sup>a</sup>, Fabienne Quilès<sup>a</sup>, Gregory Francius<sup>a</sup>, Henri-Pierre Fierobe<sup>b</sup> and  
8 Sofiane El-Kirat-Chatel<sup>a,c,\*</sup>

9  
10 <sup>a</sup> Université de Lorraine, CNRS, LCPME, F-54000 Nancy, France

11 <sup>b</sup> Laboratoire de Chimie Bactérienne (LCB), CNRS, Université d'Aix-Marseille, UMR7283 31 Chemin  
12 Joseph Aiguier, 13009 Marseille France

13 <sup>c</sup> CBMN, CNRS UMR 5248, IPB, Université de Bordeaux, Pessac, France

14  
15 \*Address correspondence to Sofiane El-Kirat-Chatel: [sofiane.el-kirat-chatel@u-bordeaux.fr](mailto:sofiane.el-kirat-chatel@u-bordeaux.fr)

16 Phone : +33-3 72 74 73 99; Fax : +33-3 83 27 54 44; Address: LCPME, 405 Rue de Vandoeuvre, 54600

17 Villers-lès-Nancy, FRANCE

18 ABSTRACT

19 Surface bacterial contamination represents a crucial health and industrial concern which requires new  
20 strategies to be continuously developed. Successful antibacterial surfaces are characterized by a  
21 combination of durable and broad-spectrum antimicrobial actions. Herein, we present a bio-inspired  
22 strategy mimicking natural cellulosome to simultaneously immobilize multiple enzymes with  
23 antibacterial activity onto surfaces. The grafting strategy leverages the strong biomolecular interaction  
24 between receptors on a scaffold protein anchored on the substrate and ligands added to the enzymes.  
25 As a proof of concept, lysozyme and lysostaphin were chosen to target the bacterial cell wall, and  
26 DNase I to degrade DNA released during cell lysis, known to promote bacterial adhesion which can  
27 later lead to biofilm formation. The specificity of the ligand/receptor interaction was confirmed by  
28 biochemical and AFM-based single-molecule force spectroscopy assays, thus demonstrating successful  
29 co-immobilization of the three enzymes on the protein scaffold. Then, the antibacterial protection was  
30 evaluated against *Staphylococcus aureus*, *Escherichia coli* and *Micrococcus luteus* by viability tests  
31 which revealed long-term antimicrobial protection of the multi-enzymatic scaffold on both Gram-  
32 positive and Gram-negative bacteria. After 24 hours of contact, the system induced lysis of 71 to 85%  
33 of bacteria, and its antimicrobial properties remained effective after 5 days even with several  
34 cumulative waves of bacterial contaminations. This work demonstrates the relevance of bio-inspired  
35 multi-enzymatic scaffolds for antibacterial protection, providing long-term and broad-spectrum action.

36 STATEMENT OF SIGNIFICANCE

37 With the raise of resistance among pathogenic bacteria, it became crucial to find alternatives to  
38 conventional antibiotics. Antimicrobial enzymes present many advantages as they are “re-usable”, less  
39 associated with resistance issues, non-toxic and can withstand a wide range of contaminations. In this  
40 article, we focus on grafting antibacterial enzymes on materials surfaces. We used a bio-inspired  
41 approach to simultaneously graft different yet complementary enzymes on a protein scaffold and to  
42 achieve broad-spectrum antibacterial effect. The resulting multi-enzymatic scaffold enhanced

43 antibacterial effects compared to a strategy where the enzymes were directly grafted on the material's  
44 surface. This was a proof of concept of antibacterial strategies bio-inspired by cellulosomes as our  
45 system provided long-lasting protection concurrently against Gram + and Gram – bacteria.

## 46 1. INTRODUCTION

47 Bacterial infections pose a significant threat in both medical and industrial contexts. They represent an  
48 ever-growing global scourge which caused the death of 7.7 million patients in 2019, about one eighth  
49 of the total number of deaths worldwide <sup>1</sup>. Infections often take the form of surface contaminations  
50 forming on medical devices such as wound dressings, urethral and intravascular catheters, prosthetic  
51 grafts, prosthetic joints, and shunts <sup>2,3</sup>. This leads to increased mortality and morbidity which causes  
52 an important economic burden on health care systems <sup>2,4-6</sup>.

53 Surface contamination starts with the initial adhesion of pioneer bacteria to the substrate which then  
54 multiply to form microcolonies and later biofilm, the most predominant and successful lifestyle of  
55 bacteria and highly resistant to external stress, including antibiotics <sup>7-9</sup>. Antibacterial effect (or contact-  
56 killing) is often used on surfaces to inactivate pioneer cells and therefore prevent infections by  
57 inhibiting bacterial growth and biofilm formation <sup>10-12</sup>. Initially, antibiotics and synthetic/natural  
58 antimicrobial peptides were considered promising candidates but the emergence of multi-resistant  
59 strains has rapidly put a curb on this prospect <sup>13,14</sup>. In this context, antimicrobial enzymes have been  
60 considered as an interesting alternative as they are less associated with resistance issues. Their activity  
61 is “re-usable” *i.e.* they can act several times provided their catalytic site is active which can ensure  
62 long-lasting antimicrobial effect. Moreover, some enzymes can withstand broad-spectrum  
63 contaminations and are non-toxic <sup>12,13,15-20</sup>.

64 In this work, we present an antimicrobial strategy based on a multi-enzymatic system bio-inspired by  
65 natural cellulosomes, which are cell-associated supramolecular structures or “nanomachines”  
66 consisting in several cellulolytic enzymes organized on a protein scaffold <sup>21,22</sup>. Enzymes displayed on  
67 cellulosomes have complementary roles that enable efficient degradation and absorption by  
68 cellulolytic bacteria of nutrients from cellulose, a highly recalcitrant polysaccharide. Our proposed bio-  
69 inspired strategy was to mimic the supramolecular organization of natural cellulosomes by  
70 simultaneously assembling three enzymes with complementary antimicrobial roles on a protein

71 scaffold grafted on material surfaces. Enzymes were chosen to favor broad-spectrum antimicrobial  
72 protection while concurrently preventing the accumulation of lysed cell debris on the surface. The first  
73 enzyme is lysozyme which cleaves the  $\beta$ -(1,4) bond between the N-acetyl-muramic acid and the N-  
74 acetyl-D-glucosamine residue of the peptidoglycan (PG) chains present in bacterial cell walls<sup>23,24</sup>. This  
75 enzyme was also reported to act against Gram-negative bacteria through membrane disruption. For  
76 instance, it has the capability to permeabilize both the outer and inner membranes of *E. coli*, achieving  
77 this effect with and without the formation of pores, respectively<sup>24-27</sup>. The second enzyme is  
78 lysostaphin, an endopeptidase that hydrolyses the pentaglycine chains linking the PG fibrils in the cell  
79 wall of staphylococci, a major pathogenic genus<sup>28</sup>. The third enzyme is deoxyribonuclease I (DNase I),  
80 which aims to degrade the extracellular DNA, an important polymer released during cell lysis by cell  
81 wall degrading enzymes, and known to promote microbial adhesion and bacterial cohesion<sup>29</sup>.

82 Immobilizing antimicrobial enzymes is a crucial and challenging step for antibacterial strategies.  
83 Ideally, the grafting technique should preserve the tridimensional conformation of the enzymes to  
84 ensure their antimicrobial effects. It should also provide an optimized accessibility of the catalytic site  
85 once loaded onto the surface. A wide range of immobilization methods rely on physical adsorption or  
86 direct covalent attachment on the substrate which often lead to steric hindrance of randomly  
87 orientated enzymes, loss of activity of antimicrobial compounds due to conformational changes and  
88 possibly leaching of adsorbed molecules<sup>13,19,30</sup>. Previously, we demonstrated that strategies based on  
89 strong-affinity biomolecular ligand/receptor interactions present many advantages for antibacterial  
90 and antibiofilm properties as they ensure a controlled orientation of the grafted enzymes<sup>30</sup>. This  
91 controlled immobilization preserves the orientation and the conformation of the enzymes and thus  
92 contributes to optimal and long-lasting antimicrobial properties. Lysozyme, for instance, was  
93 successfully grafted on a substrate and showed enhanced antimicrobial effects over several  
94 consecutive cycles of contaminations when grafted in an ordered manner, via ligand/receptor  
95 interactions, rather than randomly orientated<sup>30</sup>. Yet, this approach cannot be applied to the  
96 simultaneous and controlled grafting of several enzymes with complementary activities in order to

97 broaden the antimicrobial protection towards various contaminants. In the strategy proposed herein,  
98 chimeric ligand-tagged enzymes were grafted on receptors located on a recombinant protein scaffold,  
99 a supramolecular organization similar to those of natural cellulosomes. Cellulosomal enzymes  
100 anchored on supramolecular structures found in natural cellulosomes show optimal synergistic activity  
101 which is significantly enhanced compared to the corresponding free enzymes<sup>31</sup>. These supramolecular  
102 assembly relies on a highly specific and strong ligand/receptor interactions between domains named  
103 dockerin and cohesin, respectively<sup>32</sup>. The calcium-dependent ligand/receptor pairs in cellulosomes  
104 were found to be one of the strongest non-covalent biomolecular bonds known in nature where a  
105 duplicated calcium-binding loop-helix motif of the ligand interacts with the receptor site<sup>32-36</sup>.

106 Here we demonstrated that bio-inspired multi-enzymatic scaffold is an attractive strategy to prevent  
107 surfaces from being colonized by biofilm-forming bacteria. Far western blot based on scaffold  
108 detection confirmed that all three enzymes displayed functional dockerin modules and were  
109 successfully immobilized on the scaffold *via* ligand/receptor (dockerin/cohesin) binding. Atomic force  
110 microscopy (AFM)-based single-molecule force spectroscopy (SMFS) revealed the calcium-dependent  
111 nature of the ligand/receptor interactions used to dock the enzymes on the protein scaffold, similarly  
112 to natural cellulosome. It also demonstrated a strong binding and the specificity of these interactions.  
113 Lastly, viability assays on planktonic bacteria indicated the antimicrobial effect of the multi-enzymatic  
114 scaffold over five consecutive cycles of contamination by biofilm-forming bacteria, namely  
115 *Staphylococcus aureus*, *Escherichia coli* and *Micrococcus luteus*.

## 116 **2. MATERIALS AND METHODS**

### 117 **2.1. Reagents and proteins**

118 Lysozyme from chicken egg white (>90%, >40 units/mg), recombinant lysostaphin and DNase I (≥2,000  
119 Kunitz units/mg protein) from bovine pancreas were purchased from Sigma and BioVendor (France).  
120 Recombinant scaffold protein as well as lysozyme, lysostaphin and DNase I enzymes tagged with  
121 ligands were produced and purified by the Protein Production and Purification Plateforme of the

122 Institut de Biologie Moléculaire et Cellulaire (IBMC)-CNRS of the Université de Strasbourg (details  
123 below).

## 124 **2.2. Scaffold expression and purification**

125 BL21 (DE3) *E. coli* strain transformed with pET9d-Scaf6-6xHis plasmid was grown at 37°C and in 2L  
126 lysogeny broth medium supplemented with 1,2% glycerol and Carbenincilin until reaching an optical  
127 density of 1.5. The temperature was lowered to 20°C and the expression induced by 0.2 mM IPTG  
128 during 20 hours.

129 Bacteria were collected by centrifugation at 5000 *g*, resuspended in 50 mL of 50 mM NaPO<sub>4</sub> (pH = 7)  
130 with 20 µg/mL DNase I and protease inhibitors mix (Roche), and lysed with a Microfluidizer LM-20  
131 (Microfluidics).

132 The lysate was clarified by centrifugation at 18000 *g* for 20 min at 4°C, the supernatant collected and  
133 incubated with 15 g of micro-crystalline AvicelPH101 cellulose (SIGMA) for 90 min at 4°C under  
134 constant agitation. The cellulose was recovered by filtration on 2 µm glass fiber filter and washed three  
135 times with 50 mL of 50 mM NaPO<sub>4</sub> (pH = 7) and twice with 50 mL of 12.5 mM NaPO<sub>4</sub> (pH = 7).

136 Protein was sequentially eluted by three 50 mL volumes of cold water, followed by two sequential  
137 50 mL volumes of 1 % triethanolamine, immediately buffered by the addition of 0.1 volume of 500 mM  
138 Tris-HCl (pH = 8). Elution fractions were assessed by SDS-PAGE and those containing the protein were  
139 pooled and filtered at 0.2 µm. The protein was further purified on an Akta Pure FPLC system with a  
140 MonoQ 5/150 GL anion exchange column (Cytiva) equilibrated in 25 mM Tris-HCl (pH = 8), 10 % glycerol  
141 and eluted with a gradient 0-1M NaCl, 25mM Tris-HCl (pH = 8) and 10 % glycerol. Fractions containing  
142 Scaf6 were pooled and loaded onto a HiLoad 16/60 Superdex S200 size exclusion column (Cytiva)  
143 equilibrated in PBS (pH = 7.4). Fraction corresponding to the monomeric protein were pooled and  
144 concentrated on a Vivaspin 20 concentrator (MWCO 30kDa; Sartorius) to a final concentration of  
145 3.5 mg/mL, aliquoted, snap frozen in liquid nitrogen and stored at -80°C.

146 **2.3. Tagged-enzymes expression and purification**

147 BL21 (DE3) *E. coli* strains transformed with pT7 expression vectors bearing 6His-enzymes (lysozymes,  
148 lysostaphin, and DNase I) tagged with the ligand motifs were grown at 37°C and in 1L Terrific Broth  
149 medium supplemented with kanamycin until reaching an optical density of 2.5. The temperature was  
150 lowered to 20°C and the expression induced by 0.5 mM IPTG during 18 hours.

151 Bacteria were collected by centrifugation at 5000 *g*, resuspended in 100 mL 25mM Tris-HCl (pH = 8),  
152 150 mM NaCl, 0,1% CHAPS, 3mM  $\beta$ -mercapto-ethanol, and lysed with a Microfluidizer LM-20  
153 (Microfluidics).

154 The lysate was clarified by centrifugation at 18000 *g* for 20 min at 4°C, and the supernatant purified  
155 on an Akta Pure FPLC system by binding on a HisTrap HP Ni-NTA affinity column (Cytiva) with 25 mM  
156 imidazole. The protein was eluted by a 25 to 500 mM imidazole gradient in 25 mM Tris-HCl (pH = 8),  
157 150mM NaCl, 0,1% CHAPS, 3 mM  $\beta$ -mercapto-ethanol. Fractions enriched in tagged enzymes were  
158 further purified on a Hi-Load 16/60 Superdex 75 column (Cytiva) equilibrated in PBS (pH = 7.4).  
159 Fractions containing monomeric tagged enzymes were pooled and concentrated on an AMICON Ultra  
160 4 (MWCO 3kDa, Millipore) to a final concentration of 1.5 mg/mL, aliquoted, snap frozen in liquid  
161 nitrogen and stored at -80°C.

162 **2.4. Far western blots**

163 Ligand-tagged and non-tagged proteins (20  $\mu$ L at 0.2 mg/mL) were mixed with 6  $\mu$ L of denaturing  
164 buffer, prior boiling for 5 min. 5- $\mu$ L of boiled samples were subjected to denaturing polyacrylamide gel  
165 electrophoresis (SDS-PAGE) using Bio-rad precast gels (gradient 4-15%) and analyzed by far western  
166 blot, after transfer on nitrocellulose (GE healthcare), using biotinylated Scaf6 and streptavidin-POD  
167 (Roche) as formerly described in <sup>37</sup>.

168 **2.5. Surface and AFM tip functionalization**

169 Silicon wafers and round glass coverslips ( $\varnothing$ 12 mm) were coated by plasma sputtering with an under  
170 layer of chromium ( $\sim$ 10 nm) and an upper layer of gold ( $\sim$ 30 nm). They were then cleaned by UV-ozone  
171 treatment for 15 min, rinsed with ethanol and dried under  $N_2$  flow.

172 Enzymes and scaffolds were covalently attached on self-assembled monolayers (SAMs) of carboxyl-  
173 terminated alkanethiols. Briefly, gold-coated substrates and gold-coated NPG-D (Bruker) AFM tips  
174 were immersed overnight in a solution of 0.1 mM 16-mercaptododecahexanoic acid and 0.9 mM 11-  
175 mercapto-1-undecanol to form SAMs. They were then rinsed with ethanol and dried under  $N_2$  flow.  
176 Next, carboxylic groups were activated by immersion 30 min in a solution of N-hydroxysuccinimide  
177 (NHS, 10 mg/mL) and 1-ethyl-3-(3-dimethylaminopropyl)-carbodiimide (EDC, 25 mg/mL). AFM tips and  
178 substrates were then rinsed with ultrapure water and immersed in protein solutions (0.2 mg/mL in  
179 PBS) for 2 hours. Enzymes-decorated tips and scaffold-coated surfaces were stored in Tris-buffered  
180 saline (TBS) supplemented 1 mM  $CaCl_2$  and 1 mM  $ZnCl_2$  ( $TBS^+$ ) at 4°C for 4 days maximum before they  
181 were used for SMFS. Calcium chloride and zinc chloride were used to ensure calcium-dependent  
182 ligand/receptor interactions and zinc-dependent lysostaphin activity.

183 For bacterial viability experiments, substrates coated with scaffolds were immersed in a solution  
184 containing 0.2 mg/mL of tagged lysozyme, tagged lysostaphin and tagged DNase I. Control surfaces  
185 were prepared by grafting directly non-tagged enzymes on SAMs activated substrates (without  
186 scaffold layer) or by grafting only the scaffold (no enzyme addition). All grafting lasted for 2 hours at  
187 0.2 mg/mL in PBS. Prepared surfaces were rinsed in  $TBS^+$  and directly used for bacterial viability tests.

## 188 **2.6. AFM imaging and force spectroscopy**

189 All AFM experiments were achieved at  $21\pm 1^\circ C$  in an air-conditioned room, in  $TBS^+$  buffer using a  
190 Bioscope Resolve AFM (Bruker corporation, Santa Barbara, CA). Cantilevers spring constants were  
191 determined by the thermal noise method <sup>38</sup>. Measurement of scaffold coating thickness was  
192 performed by scanning a  $1 \times 1 \mu m^2$  area at high forces and high scan rate and then imaging a larger  
193 area (of  $5 \times 5 \mu m^2$ ) under small forces and reduced frequencies. To perform SMFS, adhesion maps of

194 32 x 32 force-distance (FD) curves on 5 x 5  $\mu\text{m}^2$  areas were recorded on the scaffold-coated substrates  
195 with the enzyme-decorated AFM tips with an applied force of 500 pN, 1  $\mu\text{m}/\text{s}$  constant approach and  
196 retraction speeds and a contact time of 500 ms. For control experiments, after acquiring adhesion in  
197 presence of calcium ( $\text{TBS}^+$ ), 20 mM of ethylenediaminetetraacetic acid (EDTA, Carlo Erba Reagents)  
198 was added in the buffer and SMFS was performed again to acquire the adhesion in the presence of the  
199 chelating agent. The media was then replaced by fresh  $\text{TBS}^+$  and SMFS was performed one last time.  
200 Positive control was achieved by performing the AFM measurements with the cellulase Cel9T from *R.*  
201 *cellulolyticum* tagged with its native dockerin.

202 The adhesion force and rupture length of the last adhesive peaks were extracted from each force curve  
203 with Nanoscope Analysis 1.8 (Bruker). Adhesion forces and rupture lengths of the last adhesive peaks  
204 for each curve were ordered in bins to form the frequencies histograms displaying adhesion  
205 frequencies and rupture frequencies. These histograms were processed with MATLAB R2016b  
206 (MathWorks) and designed in figures with Origin 2023 (OriginLab). Results presented for SMFS  
207 correspond to the average over three independent experiments of 1024 force-distance curves each.

## 208 **2.7. Bacterial growth and viability tests**

209 All bacterial cells were grown routinely at 37°C. *Staphylococcus aureus* strain 187 (HER 1239) were  
210 grown on tryptic soy broth (TSB, Sigma) plates and *Micrococcus luteus* (ATCC4698) and *Escherichia coli*  
211 (ATCC25922), on lysogeny broth Lennox (LB, Sigma) plates. For viability experiments, a single colony  
212 of *S. aureus*, *M. luteus* and *E. coli* was grown in 5 mL of respective broth media under gentle agitation  
213 (150 rpm on an agitation plate). Overnight cultures were washed twice in  $\text{TBS}^+$  by centrifugation at  
214 5000 g for 5 min before being retrieved. For the consecutive challenges, 1.2 mL of bacterial suspension  
215 containing  $\sim 5 \times 10^7$  bacteria were deposited on functionalized surfaces in 12-well plates and gently  
216 agitated at 37°C. Multiple waves of contaminations (challenges) were performed by replacing the  
217 bacterial suspension in the plates with fresh suspension containing  $\sim 5 \times 10^7$  bacteria every 24h for a  
218 total of 5 challenges. Samples were pipetted (100  $\mu\text{L}$ ) at 0h, 2h, 4h, 6h and 24h of every 24h-challenge

219 and serially diluted then plated on agar plates before culture at 37°C to determine bacterial viability  
220 by colony forming units counting. Results presented for viability tests correspond to the average on  
221 four serial dilutions for each time and over four independent experiments. Results are presented with  
222 exponential decay fittings on Origin 2023 (OriginLab).

## 223 **2.8. Statistical analysis**

224 All statistical analysis was performed using GraphPad Prism 7.0. Standard deviations of each data group  
225 of the adhesion frequency for each enzyme (n=3) were not found significantly different with a Brown-  
226 Forsythe test. A one-way ANOVA was therefore used followed by a Tukey's multicomparison test for  
227 pair-wise comparison between conditions.

## 228 **3. RESULTS**

### 229 **3.1. Ligand-tagged enzymes bound to the receptors located on the scaffolds**

230 To concurrently graft three different enzymes on surfaces, we decided to construct and purify after  
231 heterologous expression an interspecific hybrid scaffold made of receptors (cohesin modules) from  
232 three different species, namely *Acetivibrio thermocellus* (formerly known as *Clostridium*  
233 *thermocellum*), *Ruminiclostridium cellulolyticum* and *Ruminococcus flavefaciens*, and separated by  
234 spacers of 30 amino acids. Enzymes of interests were tagged with the ligands corresponding to their  
235 scaffold receptors, *i.e* lysostaphin, lysozyme and DNase I were tagged with ligands (dockerin modules)  
236 from *A. thermocellus*, *R. cellulolyticum* and *R. flavefaciens*, respectively. More precisely, Cel48S  
237 dockerin from *A. thermocellus* was anchored on the C-terminus of lysostaphin to form the tagged  
238 lysostaphin; lysozyme tagged enzymes carried Man5K dockerin from *R. cellulolyticum* on the N-  
239 terminus; and tagged DNase I was tagged with dockerin from *R. flavefaciens* on its C-terminus. The  
240 cellulase Cel9T from *R. cellulolyticum* with its native dockerin was used as positive control to confirm  
241 binding of native enzyme-ligand to scaffold receptor<sup>39</sup>. Enzymes were tagged with ligand of different  
242 species to ensure that each tagged enzyme had a specific receptor on the scaffold and thus that each  
243 enzyme could bind to the scaffold. Far western blots were the first step of our work to evaluate the

244 ability of the enzymes to bind to the scaffold. Electrophoresis gel with the tagged and non-tagged  
245 lysostaphin, lysozyme and DNase I were transferred onto a membrane and biotinylated scaffold was  
246 used to probe the membrane. Bands at 36 kDa, 23 kDa and 41 kDa were revealed and attributed to  
247 tagged lysostaphin, tagged lysozyme and tagged DNase I, respectively (Figure 1). No bands were  
248 observed when the biotinylated scaffold was used to probe non-tagged enzymes, namely lysostaphin  
249 (27 kDa), lysozyme (16 kDa) and DNase I (31 kDa). This confirmed that tagged enzymes specifically  
250 bound to the scaffold whereas non-tagged ones were unable to bind to it. Based on these results, it  
251 was assumed that, all three tagged enzymes bound to the scaffold and that the receptor located on  
252 the scaffolds targeted specifically tagged enzymes.

### 253 **3.2. Enzymes tagged with ligand interacted specifically with scaffold-coated surfaces**

254 Probing the interaction between the enzymes and scaffold-coated surfaces was a crucial step in order  
255 to demonstrate that the surface functionalization strategy led to the immobilization of tagged enzymes  
256 through specific interactions between the ligands of the enzymes and the receptors located on the  
257 scaffolds.

258 First, scaffolds were covalently grafted on material surfaces and topography AFM images were  
259 performed to confirm the grafting. In order to evaluate the thickness of the coatings, a part of each  
260 coating was removed by “scratching” a squared area of  $1 \times 1 \mu\text{m}^2$  at high forces ( $> 10 \text{ nN}$ ) and high  
261 frequencies with AFM tips. A coating was considered present on the surface of the material when a  
262 scratched square was visible on the image. The depth of the scratched area was considered an  
263 estimation of the coating thickness (Figure 2).

264 Images of surfaces coated only with SAMs revealed a smooth and flat surface on which the coating  
265 was not visible even after using the “scratching” AFM technique (Figure 2a). The relatively small size  
266 of the molecules composing the SAMs, the typical thickness of carboxylic acid terminated SAMs (few  
267 ångströms<sup>40</sup>) and the covalent nature of the coating made difficult to evidence the SAMs with the  
268 “scratching” AFM technique. However, when the scaffold was added on the SAMs-coated surfaces, the

269 resulting coating was observable on the AFM images and was homogeneous throughout the surface  
270 (Figure 2b). Its thickness was evaluated at  $1.95 \pm 0.24$  nm which confirmed that the scaffold bounded  
271 with the carboxyl groups of the SAMs. When the tagged-enzymes were added on the surface coated  
272 with the SAMs and the scaffold, the thickness of the coating increased and reached  $7.80 \pm 0.67$  nm  
273 (Figure 2c). This evidenced the binding of the enzymes' ligands onto the scaffold's receptors as the  
274 increased thickness of the coating was attributed to the addition of the tagged enzymes. When  
275 scanned in contact mode at small forces, the coatings remained stable and no visible topography  
276 alterations were observed indicating a strong anchorage of the coatings on the substrate.

277 AFM imaging and far western blots showed that the enzymes had the ability to bind to the scaffold but  
278 to investigate these bonds further, the specificity of the receptor-ligand interactions was assessed by  
279 AFM-based SMFS. For that, each enzyme was grafted one at a time on AFM cantilevers which were  
280 then used to probe scaffold-coated surfaces (Figure 3).

281 For each enzyme-decorated AFM tip, adhesion in presence of calcium was first probed on the scaffold  
282 coating by recording adhesion maps. To test the calcium-dependency of the receptor/ligand pairs, a  
283 calcium chelating agent (EDTA) was added to the buffer to trap free calcium ions and SMFS  
284 measurements were subsequently performed a second time. Lastly, EDTA was removed, the buffer  
285 containing calcium was added and adhesion was recorded for the last time.

286 Figures 4, 5 and 6 show the adhesion frequencies and the rupture lengths histograms as well as  
287 representative force-distance (FD) curves for ligand-tagged lysostaphin, lysozyme and DNase I and  
288 their corresponding negative controls, *i.e.* non-tagged enzymes. For all enzymes, adhesive pixels on  
289 adhesion maps were randomly spread and adhesion maps did not show cluster patterns (data not  
290 shown). This suggests that the scaffolds were homogeneously grafted on the surfaces which matched  
291 the results observed above with the AFM topography images (Figure 2).

292 Before adding EDTA, representative FD curves showed adhesion peaks for all ligand-tagged enzymes  
293 (Figure 4a, 5a and 6a). In contrast, less adhesion signatures were found on FD curves when EDTA was

294 added with the ligand-tagged enzymes (Figure 4b, 5b and 6b). However, once EDTA was removed,  
295 adhesion signatures were restored (Figure 4c, 5c and 6c). Little to no adhesion signature were observed  
296 on FD curves of homologous enzymes lacking ligands (Figure 4d, 5d and 6d). Adhesion frequency in  
297 presence of calcium for tagged lysostaphin was high since 86% of the FD curves showed an adhesion  
298 signature (Figure 4a). Adhesion frequency then dropped to around 42% when EDTA was added (Figure  
299 4b) and increased again to 87% after EDTA was rinsed and calcium chloride was added (Figure 4c). In  
300 contrast, only 8% of the FD curves showed adhesion signature for non-tagged lysostaphin (negative  
301 control, Figure 4d) which we attributed to non-specific adhesion events. In presence of calcium, the  
302 average adhesion frequency of tagged lysozyme was 42% (Figure 5a); it decreased to 12% with EDTA  
303 (Figure 5b) and increased to 33% when EDTA was removed (Figure 5c). Non-tagged lysozyme (negative  
304 control) adhesion frequency was 13% which shows that EDTA was able to completely inhibit  
305 ligand/receptor recognition in the case of this tagged lysozyme sample (Figure 5d). Adhesion  
306 frequencies of tagged DNase I was 61% in presence of calcium (Figure 6a), 4% when EDTA was added  
307 (Figure 6b) and 25% when EDTA was removed (Figure 6c). EDTA was also able to totally inhibit  
308 interactions for this sample since only 8% FD curves recorded with non-tagged DNase I presented  
309 adhesion peaks (Figure 6d). Adhesion forces and rupture lengths of scaffold-enzymes interactions  
310 ranged from 100 to 400 pN and 5 to 150 nm, respectively. Tagged lysostaphin, tagged lysozyme and  
311 tagged DNase I mean rupture forces, in absence of EDTA and over three independent experiments of  
312 1024 FD curves each, were on average  $211 \pm 2$  pN,  $297 \pm 4$  pN and  $246 \pm 3$  pN, respectively (results are  
313 reported as mean  $\pm$  standard error of the mean).

314 Figure 7 represents adhesion frequencies for each condition and each enzyme on three independent  
315 experiments of 1024 FD curves each. Adhesion frequencies decreased significantly for all enzymes in  
316 presence of EDTA which confirmed the calcium-dependent nature of the ligand/receptor interactions.  
317 Before EDTA addition, differences were observed in the adhesion frequencies between the tagged-  
318 enzymes. Tagged lysostaphin reached an average of  $87 \pm 4\%$  adhesion frequency whilst tagged lysozyme

319 and DNase I were around  $42\pm 4\%$  and  $61\pm 17\%$ , respectively (Figure 7). Tagged lysostaphin led to the  
320 most adhesion compared to the other tagged enzymes before and after addition of EDTA.

321 No significant differences were found between the EDTA condition and the negative control (non-  
322 tagged enzymes) for tagged lysozyme and tagged DNase I. EDTA was therefore able to entirely inhibit  
323 ligand/receptor interactions for these tagged enzymes. As for the interactions between tagged  
324 lysostaphin and the scaffold, EDTA was able to inhibit by around half of them. Since tagged lysostaphin  
325 resulted in the most adhesion compared to other tagged enzymes, EDTA not being able to inhibit all  
326 interactions for tagged lysostaphin was attributed to the high affinity of the ligand/receptor pair  
327 and/or to a limited EDTA accessibility to the calcium-binding loop-helix motif of this ligand/receptor.

328 After removal of chelating agent, tagged lysostaphin adhesion frequency was entirely restored as no  
329 significant differences were found before adding EDTA and after removal of EDTA (Figure 7). Adhesion  
330 frequencies of tagged lysozyme and tagged DNase I were significantly higher before adding EDTA than  
331 after which showed that the adhesion was partially restored after the chelating agent was removed.  
332 This partial restoration of adhesion was also observed with the positive control achieved with the  
333 natural cellulosome cellulase Cel9T from *R. cellulolyticum*. Adhesion of the positive control was  
334 inhibited by EDTA and almost half of the adhesion was restored after removal of EDTA. However, for  
335 all enzymes, after EDTA was removed, a significant increase in adhesion frequencies was observed.  
336 These results confirmed that in absence of free calcium in the buffer (*i.e.*, when EDTA was added), the  
337 ligand/receptors interactions between the tagged-enzyme and the scaffolds were inhibited and  
338 therefore that these interactions were calcium dependent.

339 Non-tagged enzymes displayed very low adhesion, compared to tagged enzymes (Figure 7). This  
340 showed the high specificity of the scaffold-enzymes interactions and this ensured that only the tagged  
341 enzymes were anchored on the scaffold and that substitution with other proteins were highly unlikely.  
342 As a result, very low adhesion observed on non-tagged enzymes were attributed to non-specific  
343 interactions.

### 344 3.3. Multi-enzymatic scaffold coating improved antimicrobial protection of surfaces

345 To assess surface protection achieved by our system, antibacterial effect was evaluated over multiple  
346 waves of contaminations (challenges) with fresh bacteria by standard plating assays. Bacteria were  
347 exposed to surfaces coated with the multi-enzymatic scaffolds. To evaluate the relevance of the  
348 scaffold in the system, results were compared to samples onto which enzymes were directly grafted  
349 without any protein scaffolding. Surfaces only coated with the scaffolds were used as negative  
350 controls. Bacterial viability was evaluated after 0h, 2h, 4h, 6h and 24h of exposition. Each 24h, the  
351 media was replaced by a fresh suspension of bacteria. The same procedure was repeated over 5  
352 consecutive days (Figure 8).

353 On the control surface, bacterial viability was around 90 to 100 % after 24h for most challenges (Figure  
354 8). Slight decreases (< 10 %) were observed over time for some samples and were attributed to: i)  
355 bacteria adhering to the plastic well plate where the surfaces were immersed and thus not being  
356 collected when performing viability assays, and/or ii) possible bacterial aggregation that reduce the  
357 number of CFU, *i.e.* one CFU could have been corresponding to aggregated bacteria instead of  
358 individual cells growing as a colony, thus artificially reducing the survival rate<sup>41</sup>.

359 The multi-enzymatic coating showed broad spectrum antimicrobial effects as both Gram-negative,  
360 namely *E. coli*, and Gram-positive bacteria, *S. aureus* and *M. luteus* were killed. Around 83 % of *S.*  
361 *aureus*, 71 % *E. coli* and 84 % of *M. luteus* cells were lysed after the first 24h when in contact with the  
362 multi-enzymatic scaffold (Figure 8a, b, c). In contrast, enzymes directly grafted on surfaces without any  
363 scaffold support had a milder effect on bacterial lysis. Around 62 % of *S. aureus* were lysed in contact  
364 with enzymes grafted directly on the surface after the first 24h (Figure 8a) and around 52 % and 46 %  
365 for *E. coli* and *M. luteus*, respectively (Figure 8b, c). Multi-enzymatic scaffolds exhibited more  
366 antimicrobial effects throughout the five consecutive challenges than enzymes grafted directly on the  
367 material surface.

368 The antibacterial effects of multi-enzymatic scaffolds remained unchanged after five consecutive  
369 challenges for *E. coli* and *M. luteus*. Around 71 % of *E. coli* bacteria were lysed at the end of the first  
370 challenge and 73 % at the end of the fifth challenge for the multi-enzymatic scaffold. *M. luteus* lysing  
371 rate varied from 84 % at 24h to 82 % at the end of the fifth challenge. A slight decrease in bacterial  
372 lysing rate was observed with *S. aureus* with the multi-enzymatic scaffold but the antimicrobial action  
373 remained high nonetheless. Around 70% of *S. aureus* were lysed by the multi-enzymatic scaffold after  
374 five consecutive challenges whereas the lysed rate was roughly 83% for the first challenge. A similar  
375 decrease in lysing rate was also observed for the unsupported enzymes for *S. aureus* dropping from  
376 62% after 24h to 45% after the fifth challenge.

#### 377 4. DISCUSSION

378 Key features of a successful protective surface reside in a long-lasting and broad-spectrum  
379 antibacterial effect. Aside from many crucial advantages in the fight against infections, antibacterial  
380 enzymes are known to be long lasting as long as their catalytic site is active in comparisons of other  
381 strategies that often relies on a “one-shot” effect<sup>12,13,15-20</sup>. However, antibacterial enzymes are specific  
382 and target a narrow range of pathogens. This presents the advantage of limiting adverse effects by  
383 avoiding the lyse of benign commensal microbiome threatened by broad spectrum antibiotics<sup>42</sup>. But,  
384 at the same time, antibacterial surface treatment composed of a single antibacterial enzyme have  
385 intrinsically a limited spectrum of action. In order to increase the range of action of the antibacterial  
386 surfaces, our bio-inspired strategy is based on the simultaneous grafting of complementary active  
387 enzymes. Previous studies showed the relevance of bi- and trifunctional chimeric scaffolds combining  
388 different cellulosomal enzymes for the construction of designer cellulosomes<sup>31,43</sup>. The proposed bio-  
389 inspired strategy was based on a similar approach to simultaneously assemble different yet  
390 complementary antibacterial enzymes on a recombinant protein scaffold. This allowed a broad-  
391 spectrum effect and a controlled positioning of each tagged enzyme on the scaffold<sup>31</sup>. Ligand/receptor

392 pairs, dockerin and cohesin respectively, from different species producing cellulosomes were used to  
393 anchor concurrently different ligand-tagged enzymes.

394 Dockerin/cohesin pairs are considered to be one of the most stable ligand/receptor interactions known  
395 with rupture forces that occurs *via* a tensile-based mechanism and above 120 pN<sup>32, 44</sup>, which is in  
396 concordance with our SMFS results. We concluded that unfolding of dockerin and cohesin which  
397 typically occurs at forces higher than 300 pN and up to 750 pN depending of the cohesin module<sup>44-46</sup>,  
398 was unlikely since such high forces were not representative of our results. The SMFS conducted in the  
399 present study showed that ligand/receptor pairs used to dock the enzymes to the scaffold were  
400 calcium-dependent similarly to ligand/receptor pairs in natural cellulosome<sup>32, 47, 48</sup>. This excluded the  
401 possibility of the tagged enzymes to be docked to the scaffold through unspecific interactions or any  
402 other interactions than through the binding of cohesin and dockerin. It also showed the highly specific  
403 interaction of our ligand/receptor strategy. The chimeric protein scaffold of our system was therefore  
404 not restricted to the anchorage of the lysozyme, lysostaphin and DNase I. As long as other enzymes of  
405 interest can be tagged with the ligand, the multienzymatic scaffold could be adapted to different  
406 applications to face other contaminants.

407 Discrepancies in adhesion frequencies of ligand and receptor interactions were observed. Tagged  
408 lysostaphin led to the highest adhesion frequencies in SMFS when in contact to its corresponding  
409 receptor on the scaffold compared to tagged lysozyme and tagged DNase I. These enhanced  
410 interaction frequencies might be attributed to species-dependent variations as it was shown that the  
411 affinity for the ligand and the receptor of *A. thermocellum* (used to bind lysostaphin to the scaffold in  
412 the present study) was higher than for ligand/receptor pairs of *R. cellulolyticum* and *R. flavefaciens*  
413 (used to dock lysozyme and DNase I, respectively, to the scaffold in our work)<sup>31</sup>. These variations in  
414 adhesion frequencies between tagged enzymes might also be explained by differences in accessibility  
415 between the ligand-tag and the receptor site and/or by a variation in steric hindrances due to the  
416 different positions of the receptors in the amino acid chain of the scaffold. The discrepancies observed

417 in rupture lengths might also have been originated from species-dependent variations, lengths of the  
418 enzymes, steric hindrances and the positioning of the receptors in the amino acid chain of the scaffold.

419 The prerequisite for long-lasting antibacterial coatings is the constant degradation of bacteria and the  
420 elimination of contaminants that can accumulate and promote biofilm formation over time. One of  
421 the major advantages of using enzymes as antimicrobial agents is that they are “reusable” and they  
422 continuously degrade bacteria as long as their catalytic site remains active. The proposed strategy  
423 combined cell wall degrading enzymes as well as DNase I which degraded DNA, an important cohesive  
424 component of the adhesion of microbial colonies and biofilm and the major polymer that would be  
425 released during cell lysis after cell wall degradation. *S. aureus* (Gram-positive), *E. coli* (Gram-negative)  
426 and *M. luteus* (Gram-positive) were chosen to assess the antimicrobial properties of the surfaces  
427 coated with the multi-enzymatic scaffolds. *S. aureus* and *E. coli* are some of the most etiologic agents  
428 in nosocomial infections <sup>2, 49, 50</sup>. Despite its typical low virulence, *M. luteus* can increase *S. aureus*  
429 pathogenesis by acting as a “proinfectious agent” and present risks of contaminations <sup>51-55</sup>. Previous  
430 studies evidenced that grafting enzymes directly on surfaces resulted in a non-oriented distribution of  
431 the enzymes <sup>29, 56-60</sup>. Supported enzymes were shown to have optimized antimicrobial activity since the  
432 orientation of their catalytic sites is improved as well as their 3D conformations <sup>30</sup>. As expected in our  
433 system, when enzymes were not supported by a scaffold, antimicrobial properties were evidenced to  
434 some extent but they were enhanced when enzymes were anchored on the supporting scaffold. The  
435 reduced efficacy of the unsupported enzymes was attributed to the randomness of their orientation  
436 on the substrate and the possible modification of their conformation leading to some of them being  
437 denatured and inactivated. The fact that consecutive challenges did not appear to alter significantly  
438 the enzymes ability to lyse bacteria whether supported or unsupported confirmed (i) the long-term  
439 “re-usable” antibacterial effect of the enzymes and (ii) the long-term properties of DNase I preventing  
440 the accumulation of lysed bacteria that are known to promote bacterial adhesion which can later lead  
441 to biofilm formation. The relevance of the use of a multi-enzymatic scaffold was confirmed throughout  
442 all the consecutive challenges since enzymes organized on the protein scaffold exhibited a higher

443 antimicrobial response compared to the enzymes grafted directly on the surfaces. The enzymes  
444 organization and immobilization on a molecular scaffold allowed a controlled orientation and better  
445 accessibility to their target and resulted in an improved protection.

## 446 5. CONCLUSIONS

447 Cellulosomes rely on a supramolecular organization to enhance enzymatic efficiency and degrade  
448 recalcitrant biopolymers. Our bio-inspired multi-enzymatic scaffold relied on a similar organization to  
449 lyse bacteria in order to protect surfaces from bacterial colony formation. Single-molecule force  
450 spectroscopy evidenced that enzymes were anchored on the scaffold through highly specific  
451 ligand/receptor interactions to form a supramolecular structure analogous to natural cellulosomes.  
452 The simultaneous use of complementary enzymes on the scaffold provided broad-spectrum protection  
453 concurrently against Gram + and Gram - bacteria. Our system exhibited substantial antimicrobial  
454 activity against planktonic biofilm forming bacteria, namely *S. aureus*, *E. coli* and *M. luteus*, by lysing  
455 71 % to 84 % of bacteria within the first 24 hours. The “re-usable” nature of the lysozyme and  
456 lysostaphin as well as the properties of DNase I ensured long term antimicrobial effects after 5  
457 consecutive 24h challenges. The scaffold improved the protective antimicrobial activity compared to  
458 unsupported enzymes. This was attributed to an optimized orientation and spatial conformation of  
459 enzymes attained with the multi-enzymatic scaffold. Enzymes were anchored on the scaffold through  
460 highly specific ligand/receptor interactions that enabled a controlled organization and positioning of  
461 the enzymes. Our system had great adaptability potential as it offered the possibility to tailor enzymes  
462 cocktails to the contamination risk of specific applications. Furthermore, considering the rapidly  
463 expanding repertoire of specific cohesin/dockerin devices described in the literature, gathering a larger  
464 number of different antimicrobial enzymes/proteins should be straightforward, whereas elongation or  
465 reduction of the inter-cohesins linkers in the scaffold could help gaining efficiency.

## 466 CONFLICTS OF INTEREST

467 Conflicts of interest: none.

468 **ACKNOWLEDGEMENTS**

469 The authors would like to thank Nicolas Baumberger and Laurence Herrgott from the Protein  
470 Production and Purification Plateforme of the Institut de Biologie Moléculaire et Cellulaire (IBMC)-  
471 CNRS of the Université de Strasbourg for the protein expression and purification. We would like to  
472 acknowledge the spectroscopy and microscopy Service Facility SMI of LCPME (Université de Lorraine-  
473 CNRS– <http://www.lcpme.ul.cnrs.fr>). This work was supported by the French National Agency for  
474 Research ANR JCJC, grant ANR-20-CE06-0001.

475 **AUTHOR CONTRIBUTIONS**

476 BA, FQ, GF, HPF and SEKC designed the research and wrote the manuscript; BA, CR, FQ, HPF and SEKC  
477 contributed to the acquisition, analysis, and interpretation of the data. BA, FQ, HPF and SEKC revised  
478 the paper and all authors approved the final version.

- 480 1. K. S. Ikuta, L. R. Swetschinski, G. R. Aguilar, F. Sharara, T. Mestrovic, A. P. Gray, N. D. Weaver,  
481 E. E. Wool, C. Han and A. G. Hayoon, *The Lancet*, 2022, **400**, 2221-2248.
- 482 2. M. Shirtliff, J. G. Leid and M. Shirtliff, *The role of biofilms in device-related infections*, Springer,  
483 2009.
- 484 3. S. Percival, *Journal of British Surgery*, 2017, **104**, e85-e94.
- 485 4. E. M. Padegimas, M. Maltenfort, M. L. Ramsey, G. R. Williams, J. Parvizi and S. Namdari, *Journal*  
486 *of shoulder and elbow surgery*, 2015, **24**, 741-746.
- 487 5. A. Premkumar, D. A. Kolin, K. X. Farley, J. M. Wilson, A. S. McLawhorn, M. B. Cross and P. K.  
488 Sculco, *The Journal of Arthroplasty*, 2021, **36**, 1484-1489. e1483.
- 489 6. M. Assefa and A. Amare, *Infect Drug Resist*, 2022, **15**, 5061-5068.
- 490 7. H.-C. Flemming and J. Wingender, *Nature reviews microbiology*, 2010, **8**, 623-633.
- 491 8. M. Otto, *Bacterial biofilms*, 2008, DOI: <https://doi.org/10.1007/978-3-540-75418-3>, 207-228.
- 492 9. K. Sauer, P. Stoodley, D. M. Goeres, L. Hall-Stoodley, M. Burmølle, P. S. Stewart and T.  
493 Bjarnsholt, *Nature Reviews Microbiology*, 2022, **20**, 608-620.
- 494 10. H.-C. Flemming, *Water Res.*, 2020, **173**, 115576.
- 495 11. D. Campoccia, L. Montanaro and C. R. Arciola, *Biomaterials*, 2013, **34**, 8533-8554.
- 496 12. I. Francolini and G. Donelli, *FEMS Immunology & Medical Microbiology*, 2010, **59**, 227-238.
- 497 13. K. Glinel, P. Thebault, V. Humblot, C.-M. Pradier and T. Jouenne, *Acta Biomater.*, 2012, **8**, 1670-  
498 1684.
- 499 14. S. Tambe, L. Sampath and S. Modak, *J. Antimicrob. Chemother.*, 2001, **47**, 589-598.
- 500 15. D. Alves and M. Olivia Pereira, *Biofouling*, 2014, **30**, 483-499.
- 501 16. A. K. Muszanska, H. J. Busscher, A. Herrmann, H. C. van der Mei and W. Norde, *Biomaterials*,  
502 2011, **32**, 6333-6341.
- 503 17. A. Shah, J. Mond and S. Walsh, *Antimicrob Agents Chemother*, 2004, **48**, 2704-2707.
- 504 18. J. J. Swartjes, P. K. Sharma, T. G. van Kooten, H. C. van der Mei, M. Mahmoudi, H. J. Busscher  
505 and E. T. Rochford, *Curr Med Chem*, 2015, **22**, 2116-2129.
- 506 19. C. Von Eiff, B. Jansen, W. Kohnen and K. Becker, *Drugs*, 2005, **65**, 179-214.
- 507 20. X. Wu, K. Fraser, J. Zha and J. S. Dordick, *ACS Appl Mater Interfaces*, 2018, **10**, 36746-36756.
- 508 21. R. H. Doi and A. Kosugi, *Nature reviews microbiology*, 2004, **2**, 541-551.
- 509 22. E. A. Bayer, L. J. Shimon, Y. Shoham and R. Lamed, *Journal of structural biology*, 1998, **124**,  
510 221-234.
- 511 23. V. M. Dillon, 2014.
- 512 24. M. Derde, V. Vié, A. Walrant, S. Sagan, V. Lechevalier, C. Guérin-Dubiard, S. Pezennec, M. F.  
513 Cochet, G. Paboeuf and M. Pasco, *Biopolymers*, 2017, **107**, e23040.
- 514 25. M. Derde, V. r. Lechevalier, C. Guérin-Dubiard, M.-F. o. Cochet, S. Jan, F. Baron, M. Gautier, V.  
515 r. Vié and F. o. Nau, *J. Agric. Food Chem.*, 2013, **61**, 9922-9929.
- 516 26. A. Pellegrini, U. Thomas, R. von Fellenberg and P. Wild, *J Appl Bacteriol*, 1992, **72**, 180-187.
- 517 27. A. Pellegrini, U. Thomas, P. Wild, E. Schraner and R. von Fellenberg, *Microbiol. Res.*, 2000, **155**,  
518 69-77.
- 519 28. J. K. Kumar, *Appl. Microbiol. Biotechnol.*, 2008, **80**, 555-561.
- 520 29. J. J. Swartjes, T. Das, S. Sharifi, G. Subbiahdoss, P. K. Sharma, B. P. Krom, H. J. Busscher and H.  
521 C. van der Mei, *Advanced Functional Materials*, 2013, **23**, 2843-2849.
- 522 30. A. Beaussart, C. Retourney, F. Quilès, R. D. S. Morais, C. Gaiani, H.-P. Fiérobe and S. El-Kirat-  
523 Chatel, *J. Colloid Interface Sci.*, 2021, **582**, 764-772.
- 524 31. H.-P. Fierobe, F. Mingardon, A. Mechaly, A. Bélaïch, M. T. Rincon, S. Pages, R. Lamed, C. Tardif,  
525 J.-P. Bélaïch and E. A. Bayer, *J. Biol. Chem.*, 2005, **280**, 16325-16334.
- 526 32. S. W. Stahl, M. A. Nash, D. B. Fried, M. Slutzki, Y. Barak, E. A. Bayer and H. E. Gaub, *Proceedings*  
527 *of the National Academy of Sciences*, 2012, **109**, 20431-20436.

- 528 33. S. D. Jeon, J. E. Lee, S. J. Kim, S. W. Kim and S. O. Han, *Biosensors Bioelectron.*, 2012, **35**, 382-  
529 389.
- 530 34. K. Sakka, Y. Sugihara, S. Jindou, M. Sakka, M. Inagaki, K. Sakka and T. Kimura, *FEMS Microbiol.*  
531 *Lett.*, 2011, **314**, 75-80.
- 532 35. M. A. Jobst, L. F. Milles, C. Schoeler, W. Ott, D. B. Fried, E. A. Bayer, H. E. Gaub and M. A. Nash,  
533 *Elife*, 2015, **4**, e10319.
- 534 36. A. L. Carvalho, F. M. Dias, T. Nagy, J. A. Prates, M. R. Proctor, N. Smith, E. A. Bayer, G. J. Davies,  
535 L. M. Ferreira and M. J. Romão, *Proceedings of the National Academy of Sciences*, 2007, **104**,  
536 3089-3094.
- 537 37. J. Ravachol, R. Borne, I. Meynial-Salles, P. Soucaille, S. Pages, C. Tardif and H. P. Fierobe,  
538 *Biotechnol Biofuels*, 2015, **8**, 114.
- 539 38. J. L. Hutter and J. Bechhoefer, *Review of scientific instruments*, 1993, **64**, 1868-1873.
- 540 39. J. Ravachol, R. Borne, C. Tardif, P. de Philip and H.-P. Fierobe, *J. Biol. Chem.*, 2014, **289**, 7335-  
541 7348.
- 542 40. M. Carot, V. Macagno, P. Paredes-Olivera and E. Patrino, *The Journal of Physical Chemistry C*,  
543 2007, **111**, 4294-4304.
- 544 41. P. Herman-Bausier, S. El-Kirat-Chatel, T. J. Foster, J. A. Geoghegan and Y. F. Dufrêne, *MBio*,  
545 2015, **6**, e00413-00415.
- 546 42. A. Langdon, N. Crook and G. Dantas, *Genome medicine*, 2016, **8**, 1-16.
- 547 43. H. P. Fierobe, E. A. Bayer, C. Tardif, M. Czjzek, A. Mechaly, A. Belaich, R. Lamed, Y. Shoham and  
548 J. P. Belaich, *J. Biol. Chem.*, 2002, **277**, 49621-49630.
- 549 44. M. Gunnoo, P. A. Cazade, A. Galera-Prat, M. A. Nash, M. Czjzek, M. Cieplak, B. Alvarez, M.  
550 Aguilar, A. Karpol and H. Gaub, *Advanced materials*, 2016, **28**, 5619-5647.
- 551 45. A. Galera-Prat, S. Morais, Y. Vazana, E. A. Bayer and M. Carrión-Vázquez, *J. Biol. Chem.*, 2018,  
552 **293**, 7139-7147.
- 553 46. A. Valbuena, J. Oroz, R. Hervás, A. M. Vera, D. Rodríguez, M. Menéndez, J. I. Sulkowska, M.  
554 Cieplak and M. Carrión-Vázquez, *Proceedings of the National Academy of Sciences*, 2009, **106**,  
555 13791-13796.
- 556 47. S. Pagès, A. Bélaïch, J. P. Bélaïch, E. Morag, R. Lamed, Y. Shoham and E. A. Bayer, *Proteins:*  
557 *Structure, Function, and Bioinformatics*, 1997, **29**, 517-527.
- 558 48. M. T. Rincón, J. C. Martin, V. Aurilia, S. I. McCrae, G. J. Rucklidge, M. D. Reid, E. A. Bayer, R.  
559 Lamed and H. J. Flint, *J. Bacteriol.*, 2004, **186**, 2576-2585.
- 560 49. G. Sharma, S. Sharma, P. Sharma, D. Chandola, S. Dang, S. Gupta and R. Gabrani, *J. Appl.*  
561 *Microbiol.*, 2016, **121**, 309-319.
- 562 50. A. Reisner, M. Maierl, M. Jörger, R. Krause, D. Berger, A. Haid, D. Tesic and E. L. Zechner, *J.*  
563 *Bacteriol.*, 2014, **196**, 931-939.
- 564 51. E. Boldock, B. G. Surewaard, D. Shamarina, M. Na, Y. Fei, A. Ali, A. Williams, E. J. Pollitt, P.  
565 Szkuta and P. Morris, *Nature microbiology*, 2018, **3**, 881-890.
- 566 52. R. Peces, E. Gago, F. Tejada, A. Lares and J. Alvarez-Grande, *Nephrology, dialysis,*  
567 *transplantation: official publication of the European Dialysis and Transplant Association-*  
568 *European Renal Association*, 1997, **12**, 2428-2429.
- 569 53. U. Dürst, E. Bruder, L. Egloff, J. Wüst, J. Schneider and H. Hirzel, *Zeitschrift für Kardiologie*,  
570 1991, **80**, 294-298.
- 571 54. G. Rodriguez-Nava, A. Mohamed, M. A. Yanez-Bello and D. P. Trelles-Garcia, *IDCases*, 2020, **20**,  
572 e00743.
- 573 55. H. Seifert, M. Kaltheuner and F. Perdreau-Remington, *Zentralblatt für Bakteriologie*, 1995, **282**,  
574 431-435.
- 575 56. D. Alves, A. Magalhães, D. Grzywacz, D. Neubauer, W. Kamysz and M. O. Pereira, *Acta*  
576 *Biomater.*, 2016, **44**, 313-322.
- 577 57. G. Yeroslavsky, O. Girshevitz, J. Foster-Frey, D. M. Donovan and S. Rahimpour, *Langmuir*, 2015,  
578 **31**, 1064-1073.

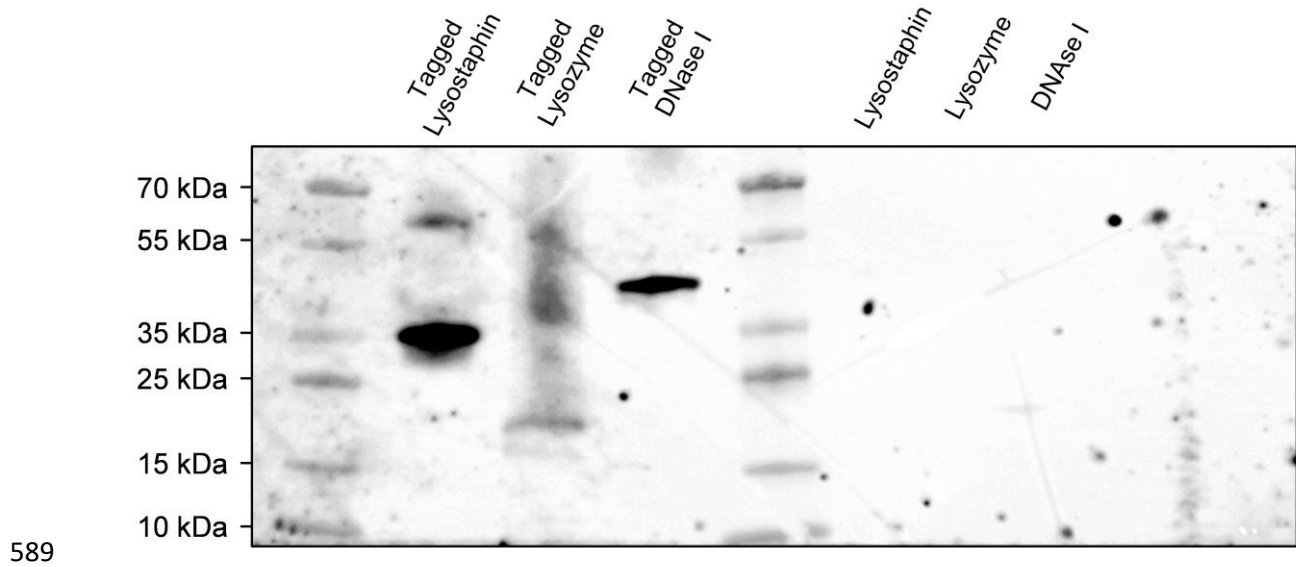
- 579 58. A. Caro, V. Humblot, C. Méthivier, M. Minier, L. Barbes, J. Li, M. Salmain and C.-M. Pradier, *J.*  
580 *Colloid Interface Sci.*, 2010, **349**, 13-18.
- 581 59. A. Caro, V. Humblot, C. Méthivier, M. Minier, M. Salmain and C.-M. Pradier, *The journal of*  
582 *physical chemistry B*, 2009, **113**, 2101-2109.
- 583 60. M. Minier, M. Salmain, N. Yacoubi, L. Barbes, C. Méthivier, S. Zanna and C.-M. Pradier,  
584 *Langmuir*, 2005, **21**, 5957-5965.

585

586

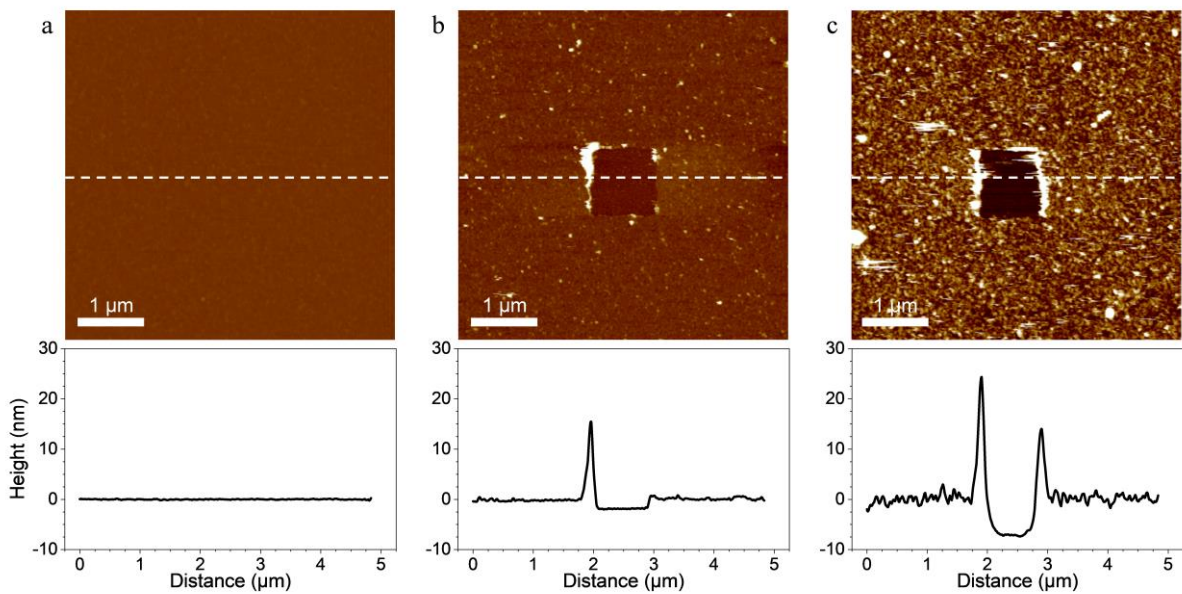
587

588



590 **Figure 1.** Far western blot using biotinylated scaffold (and Streptavidin-POD) to probe the membrane.  
 591 Tagged lysostaphin, tagged lysozyme, tagged DNase I (left channels) were identified at 36 kDa, 23 kDa  
 592 and 41 kDa, respectively. Non-tagged lysostaphin, lysozyme and DNase I (right channels) did not lead  
 593 to any interaction with biotinylated scaffold as no bands were identified.

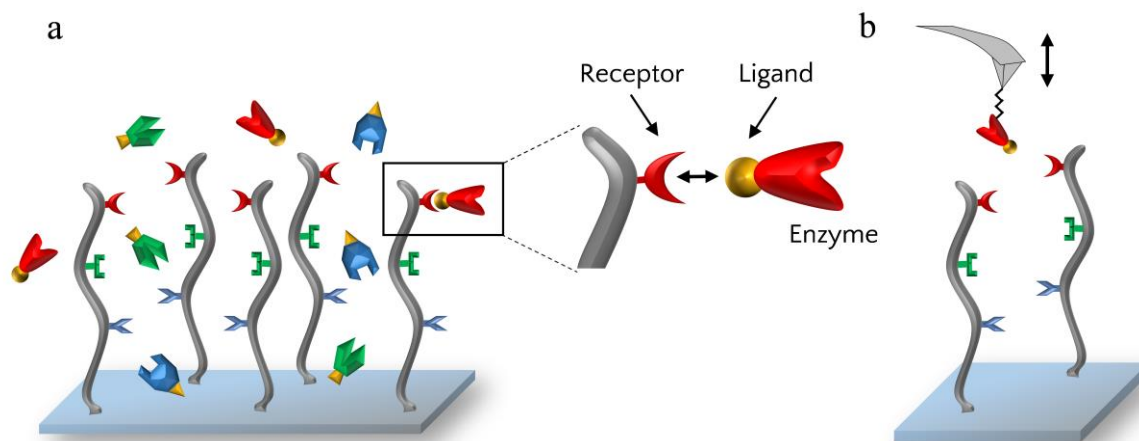
594



595

596 **Figure 2.** Topography of surfaces coated with (a) self-assembled monolayers (SAMs) only (b) SAMs and  
 597 scaffold and (c) SAMs, scaffold and the three tagged enzymes. AFM height images ( $5 \times 5 \mu\text{m}^2$ ; z values  
 598 represented by the LUT with a difference of 40 nm between the maximum and the minimum values).  
 599 A square of  $1 \times 1 \mu\text{m}^2$  was first scanned at high forces ( $> 10 \text{ nN}$ ), then, the same area was imaged ( $5 \times$   
 600  $5 \mu\text{m}^2$ ) with smaller forces. No scratched area was observed with the SAMs-coated surface. The AFM  
 601 image revealed smooth and homogenous coatings of the surface with the scaffold and the scaffold  
 602 coupled with the tagged enzymes. Scratched areas were observed and the thickness of the scaffold  
 603 coating and scaffold+enzymes coating were evaluated at  $1.95 \pm 0.24 \text{ nm}$  and  $7.80 \pm 0.67 \text{ nm}$ ,  
 604 respectively by taking a vertical section (showed below the AFM images) along the dashed line drawn  
 605 on the AFM image.

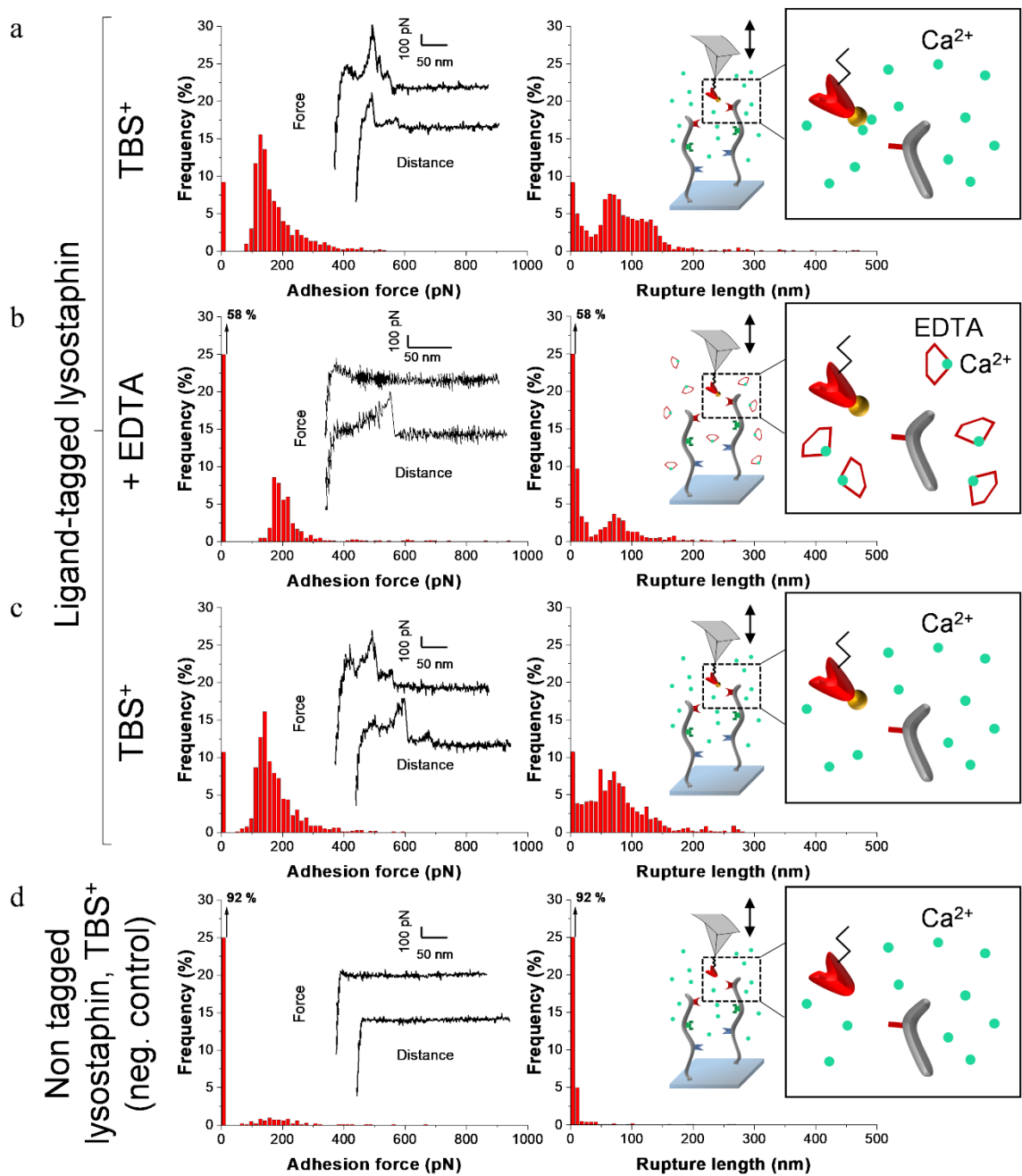
606



607

608 **Figure 3.** (a) Principle of enzyme grafting on scaffold-coated surfaces via the ligand-receptor  
 609 interaction. (b) Principle of single-molecule force spectroscopy to probe the interaction and specificity  
 610 between ligand-enzymes and receptors.

611

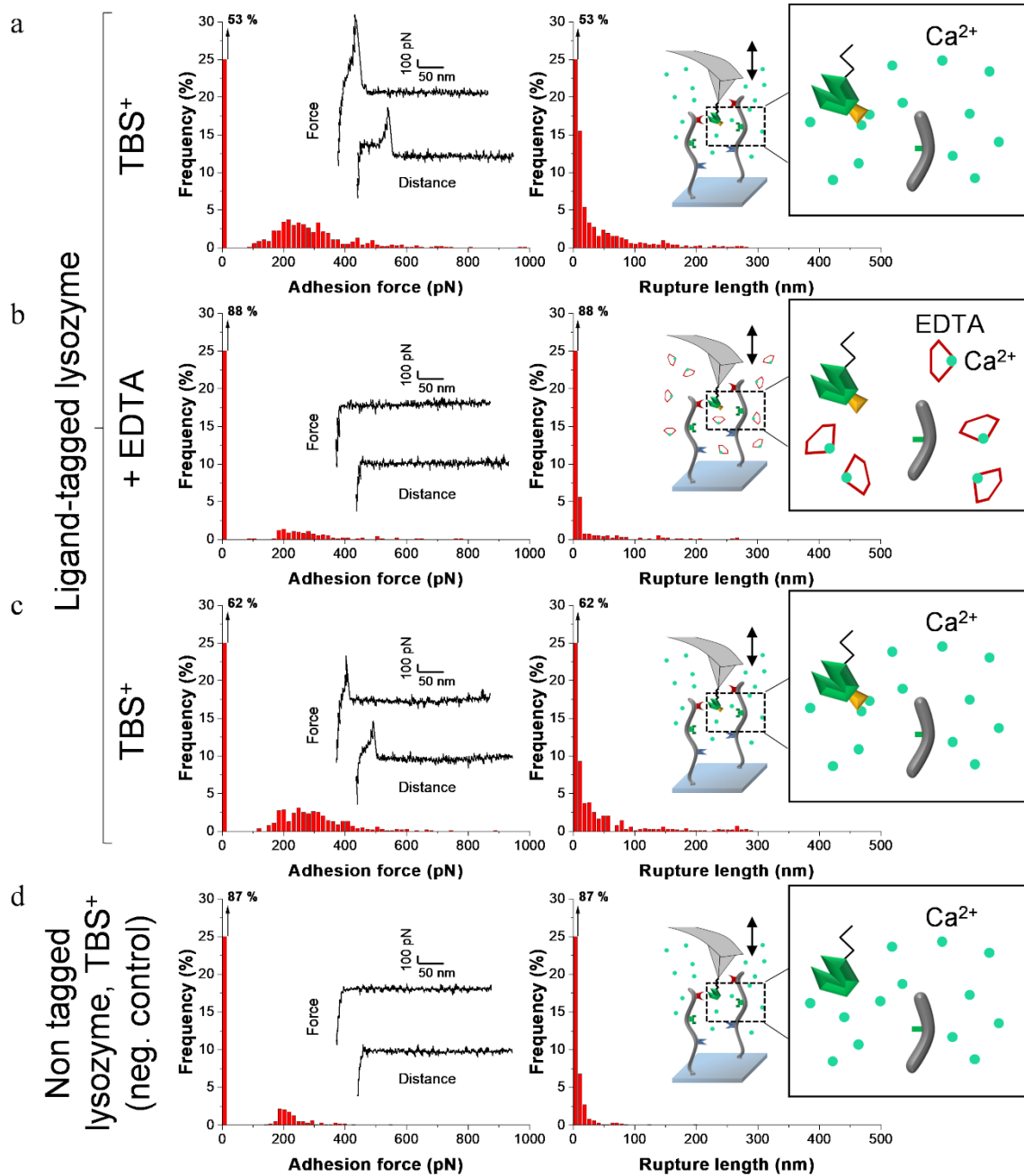


612

613 **Figure 4.** Adhesion frequency histograms with representative force curves (left) and corresponding  
 614 rupture length histograms (right) extracted from adhesion maps ( $5 \times 5 \mu\text{m}^2$ ) recorded on scaffold-  
 615 coated surfaces with AFM cantilever decorated with tagged lysostaphin. Schematics on the right  
 616 represent the different conditions: adhesion was consecutively recorded on one sample (a) in a calcium  
 617 rich buffer before adding EDTA, (b) in presence of EDTA and (c) after removal of EDTA and addition of

618 TBS<sup>+</sup> containing calcium. (d) Negative control adhesion was recorded in TBS<sup>+</sup> with tips decorated with  
619 lysostaphin lacking dockerin ligand.

620

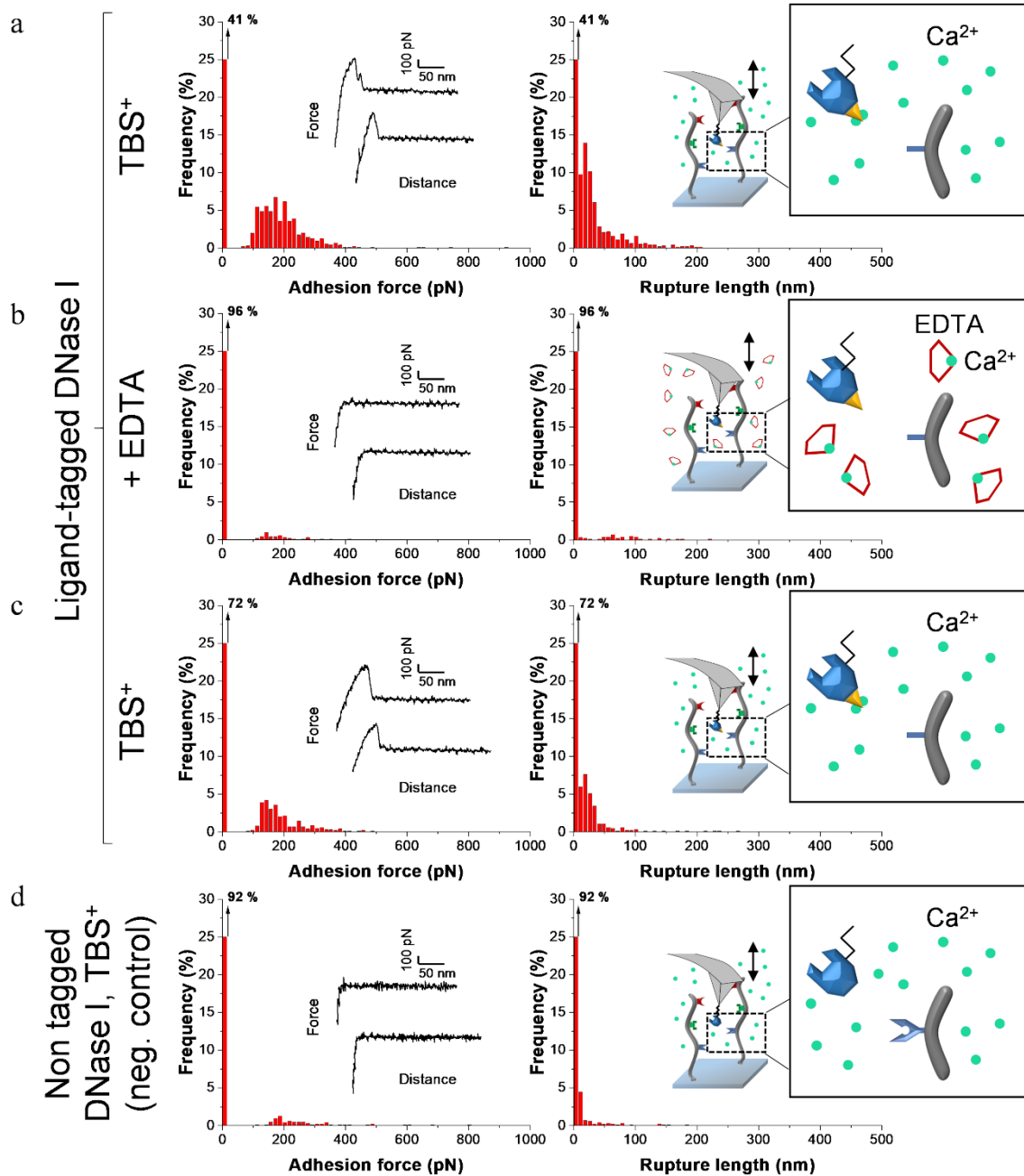


621

622 **Figure 5.** Adhesion frequency histograms with representative force curves (left) and corresponding  
 623 rupture length histograms (right) extracted from adhesion maps ( $5 \times 5 \mu\text{m}^2$ ) recorded on scaffold-  
 624 coated surfaces with AFM cantilever decorated with tagged lysozyme. Schematics on the right  
 625 represent the different conditions: adhesion was consecutively recorded on one sample (a) in a calcium  
 626 rich buffer before adding EDTA, (b) in presence of EDTA and (c) after removal of EDTA and addition of

627 TBS<sup>+</sup> containing calcium. (d) Negative control adhesion was recorded in TBS<sup>+</sup> with tips decorated with  
628 lysozyme lacking dockerin ligand.

629



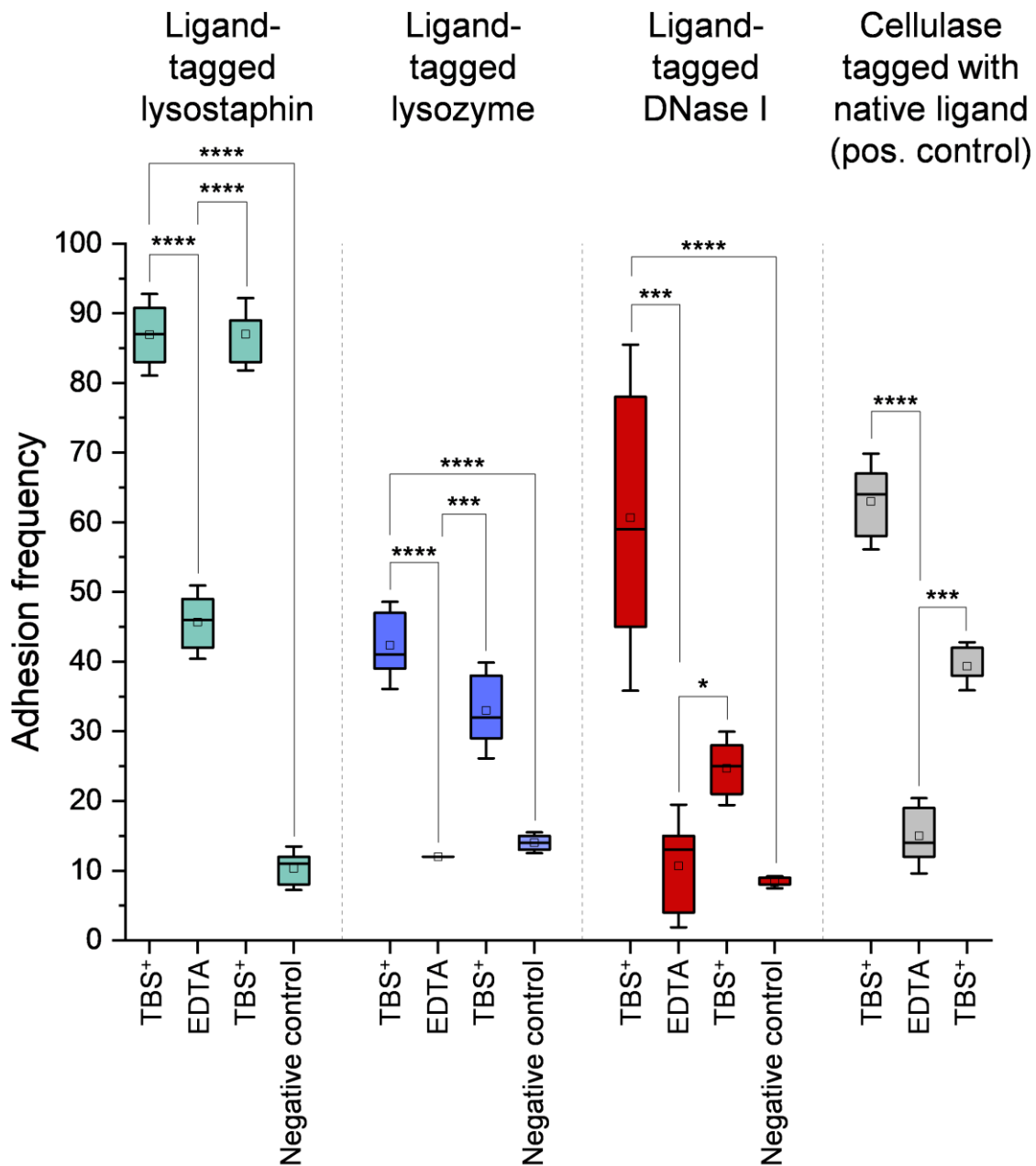
630

631 **Figure 6.** Adhesion frequency histograms with representative force curves (left) and corresponding  
 632 rupture length histograms (right) extracted from adhesion maps (5x5 μm<sup>2</sup>) recorded on scaffold-  
 633 coated surfaces with AFM cantilever decorated with tagged DNase I. Schematics on the right represent  
 634 the different conditions: adhesion was consecutively recorded on one sample (a) in a calcium rich  
 635 buffer before adding EDTA, (b) in presence of EDTA and (c) after removal of EDTA and addition of TBS<sup>+</sup>

636 containing calcium. (d) Negative control adhesion was recorded in TBS<sup>+</sup> with tips decorated with DNase

637 I lacking dockerin ligand.

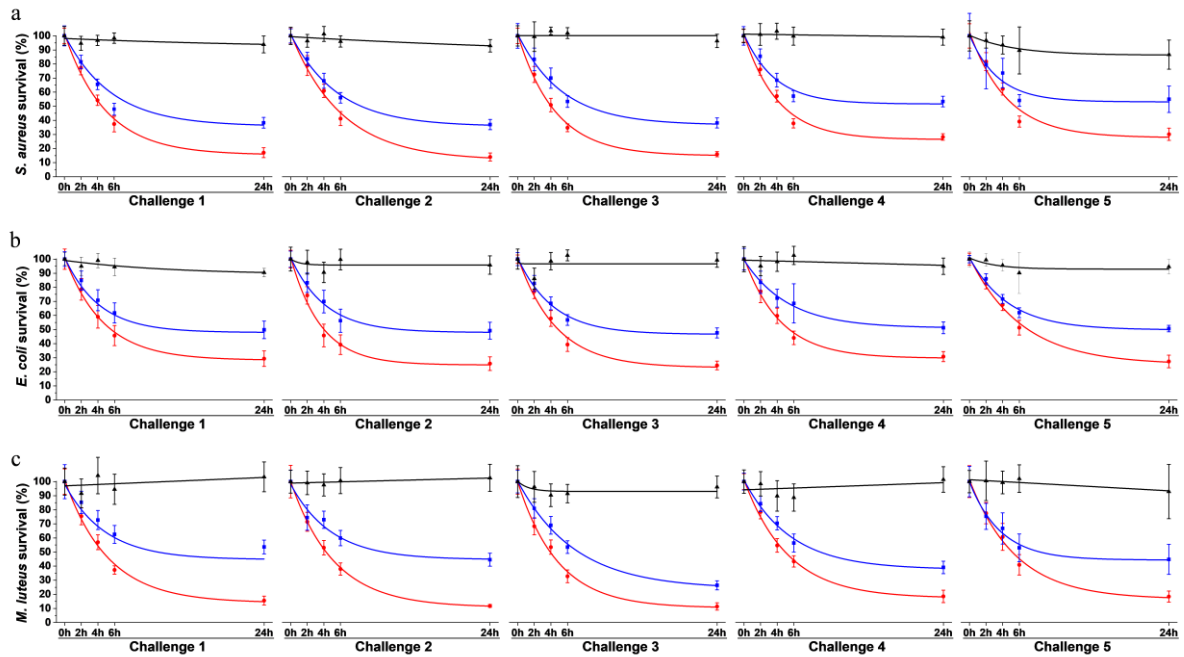
638



639

640 **Figure 7.** Adhesion frequency for each enzyme obtained by scanning the scaffold by SMFS with  
 641 enzyme-decorated AFM tips. Boxes represent the 25%-75% percentiles, error bars represent mean  $\pm$   
 642 1.5 SD and horizontal bars represent the median of each group. Each box represents 3072 force-  
 643 distance curves (n=3). Statistical analysis was performed with a one-way ANOVA followed by a Tukey's  
 644 multicomparison test for pair-wise comparison. \*:  $p < 0.05$ , \*\*:  $p < 0.01$ , \*\*\*:  $p < 0.001$ , \*\*\*\*:  $p <$   
 645 0.0001.

646



647

648 **Figure 8.** Viability of (a) *S. aureus*, (b) *E. coli* and (c) *M. luteus* exposed to surfaces coated with the  
 649 scaffold alone (in black), with the three enzymes directly on the surface without any scaffolds (in blue)  
 650 and with the multi-enzymatic scaffolds *i.e.* the three enzymes docked on the scaffolds (in red).  
 651 Challenge represent consecutive waves of bacterial contamination. Each challenge started with the  
 652 replacement of the media with fresh bacterial suspensions. Data was fitted with exponential decays.

653